



Article

Late-Holocene Sediment Storage in Upland Valley Systems in the Gamo Highlands of Southern Ethiopia

Alemayehu Kasaye Tilahun^{1,2,3,*}, Gert Verstraeten², Margaret Chen³, Guchie Gulie¹, Femke Augustijns² and Ward Swinnen²

¹ Institute of Water Technology, Faculty of Water Resources and Irrigation Engineering, Arba Minch University, Arba Minch 21, Ethiopia

² Division of Geography and Tourism, Earth and Environmental Sciences, KU Leuven, 3001 Leuven, Belgium

³ Hydrology and Hydraulic Engineering, Vrije Universiteit Brussel, 1050 Brussels, Belgium

* Correspondence: alemayehu.kasaye.tilahun@vub.be or kasayealemayehu906@gmail.com

Abstract: Part of the eroded soil material from the hillslopes is temporarily stored on hillslopes and in river valleys as colluvial and alluvial storage, respectively. This storage component of a catchment's sediment budget is an important archive reflecting past erosion and sediment delivery processes in relation to both natural and anthropogenic environmental changes. Information on long-term sediment dynamics (i.e., centennial to millennial timescales) is generally lacking for tropical mountain environments. Here, we quantify long-term floodplain sediment storage and sedimentation dynamics in the Gamo highlands of the southern Ethiopia Rift Valley. In two upstream catchments (Chencha and Dembelle), a detailed survey of the floodplain sediment archive was conducted through hand augering of 37 cross-valley transects. Sediment thicknesses vary between 4 and 8 m and total storage equals 0.03 Mt ha⁻¹ floodplain area for the Chencha area and 0.05 Mt ha⁻¹ floodplain area for the Dembelle area. Radiocarbon dating of organic material retrieved from the sediment archives provided a temporal framework for interpretation of sedimentation processes dynamic. The mean sedimentation rate in the Chencha floodplain is $\sim 3.22 \pm 0.33$ kt ha⁻¹ catchment area, whereas it is $\sim 3.76 \pm 0.22$ kt ha⁻¹ catchment area for the Dembelle floodplain. Up to 70% of the total sediment mass is stored in the floodplains within the most recent 2000 years. Cumulative probability function plots of radiocarbon dates show that sedimentation started to increase from ca 2000 to ca 1600 cal BP, roughly coincident with an increase in human presence, as is indicated through archaeological data.

Keywords: floodplain; sediment storage; long-term sedimentation rate; Ethiopia



Citation: Tilahun, A.K.; Verstraeten, G.; Chen, M.; Gulie, G.; Augustijns, F.; Swinnen, W. Late-Holocene Sediment Storage in Upland Valley Systems in the Gamo Highlands of Southern Ethiopia. *Quaternary* **2022**, *5*, 46. <https://doi.org/10.3390/quat5040046>

Received: 8 September 2022

Accepted: 28 October 2022

Published: 4 November 2022

Publisher's Note: MDPI stays neutral with regard to jurisdictional claims in published maps and institutional affiliations.



Copyright: © 2022 by the authors. Licensee MDPI, Basel, Switzerland. This article is an open access article distributed under the terms and conditions of the Creative Commons Attribution (CC BY) license (<https://creativecommons.org/licenses/by/4.0/>).

1. Introduction

Not all the sediment that is being eroded from the hillslopes is delivered to the outlet of the catchment but is stored along its pathways in the valleys systems [1–5]. Hence, sediment deposits, which are controlled by the physiographic setting of a catchment, are the main archives of the past geomorphological processes and a proxy for long-term environmental change [6,7]. Quantitative estimation of this storage component is of great importance to understand the past and present-day relations between driving forces (i.e., climate and humans) and the environment [2].

Instrumental observation of sediment transport rate at a catchment scale has resulted in a better understanding of contemporary sediment transport [8]. Information on such data has a crucial effect in sediment management strategies, building of consistent sediment budgets [9] and enhanced sediment rate models [10], which are assisting the knowledge of sediment yield in terms of environmental changes in the fluvial systems over short time periods (i.e., decades or a century) [11,12]. Whilst much data is available on contemporary erosion and sediment processes, there is for many regions a lack of understanding of the rates of these geomorphic processes in the past. Nevertheless, longer timescale (centuries

to millennia) information would be important in evaluating the current sediment dynamics pattern in terms of their historical context and in understanding the consequence of the contemporary environmental changes [13]. Most studies of long-term geomorphic processes emphasize on the investigation of different sedimentary records found in depositional environments, such as lakes, reservoirs and river floodplains. For instance, river floodplain sediment storage has been widely used to reconstruct the significance of past environmental changes on sediment dynamics [2,14–16]. It is apparent from different studies that over the time scale of centuries to millennia, river systems play an important role in transporting sediment, while floodplain sedimentation often account for a significant portion of the overall eroded sediments (up to 13%) [17,18]. Hence, from this storage, the phases with higher and lower sediment dynamics can be identified and linked to driving forces, while driving forces are primarily influencing the variability in rates of sediment processes, storage, and transport within a catchment [19–21]. Many results are available on long-time floodplain sediment storage and dynamics from case studies of various hilly and river catchments of temperate and Mediterranean regions, but less for tropical regions. Nevertheless, also in tropical mountain catchments, such as in the Ethiopian Highlands, there are many traces of human impact on vegetation going back several thousand years [21,22]. In addition, in the Gamo highlands of southwestern Ethiopia, archaeological evidence is pointing to human activities already 6500 years ago [23]. However, there is no detailed evidence on when exactly agricultural activity was introduced in the region, nor whether these early activities already had an impact on erosion and sediment transport.

Therefore, the objectives of this study are to quantify sediment storage and to understand its dynamics in the floodplain of two tropical highlands rivers in the Ethiopian Rift Valley system by establishing a chronology of sediment depositions. The floodplain sedimentation rates are analyzed over the identified timescales, whilst cumulative frequency distributions of ^{14}C -ages obtained on Holocene fluvial units are compiled and analyzed to gain more insight into the timing of floodplain sediment dynamics.

2. Materials and Methods

2.1. Study Area

This study focusses on the uplands of Elgo and Baso rivers in the Gamo highland area in SW Ethiopia (Figure 1). Both river catchments drain toward the Southern Ethiopian Rift Valley in general and Lake Chamo and Lake Abaya, respectively, in particular. The altitude in the catchment ranges from 1107 to 3500 m above sea level (m.a.s.l.). Whilst the upper parts of the catchment are characterized by an undulating plateau and gently sloping valley systems, the majority of the catchment is dominated by deeply incised river valleys and steep slopes limiting the opportunities for sediment storage, except from some localized depressions, often of tectonic origin [24]. In this study, we focus the analysis of sediment storage to these particular valley systems where sediment storage is possible (Figures 1 and 2).

Within the Elgo catchment, we focus on the floodplains in the large Dembelle depression at approx. 1450 m.a.s.l., whilst in the headwaters of the Baso river catchments we focus on the Chencha plateau at an elevation of 2800–3200 m.a.s.l. The Chencha plateau comprises of several small floodplains including Chacharo, Gossira, Olla and Tseda floodplains along the small tributaries in the headwater of the catchment. The width of the floodplains varies between 20 and 105 m in downstream direction in the Chencha study site, whereas in the Dembelle depression, valley width ranges between 300 and 2000 m. The floodplains are poorly drained and used for grassland in Chencha, while most of the Dembelle floodplain has been drained and is currently utilized for agricultural purposes.

In the Dembelle catchment, the area has been intensively deforested, and it is now dominated by cropland, with some dispersed tree patches mainly on the steeper slopes in the catchment. However, in the Chencha catchment top fertile soil has highly been degraded and now the catchment is partly converted to grassland with some planted eucalyptus trees around the farmland and home gardens. Population in the catchments

is concentrated typically on the highland part of the catchments. The local climate is dominated by the seasonal migration of the Inter-tropical convergence zone resulting in bimodal rainfall pattern. The rainy season extends from April to November accounting approximately 85% of mean annual rainfall depths. The mean annual rainfall ranges from 760 mm at the rift valley floor to 1100 mm in the highlands, whereas the temperature varies from 25 °C to 10 °C, respectively.

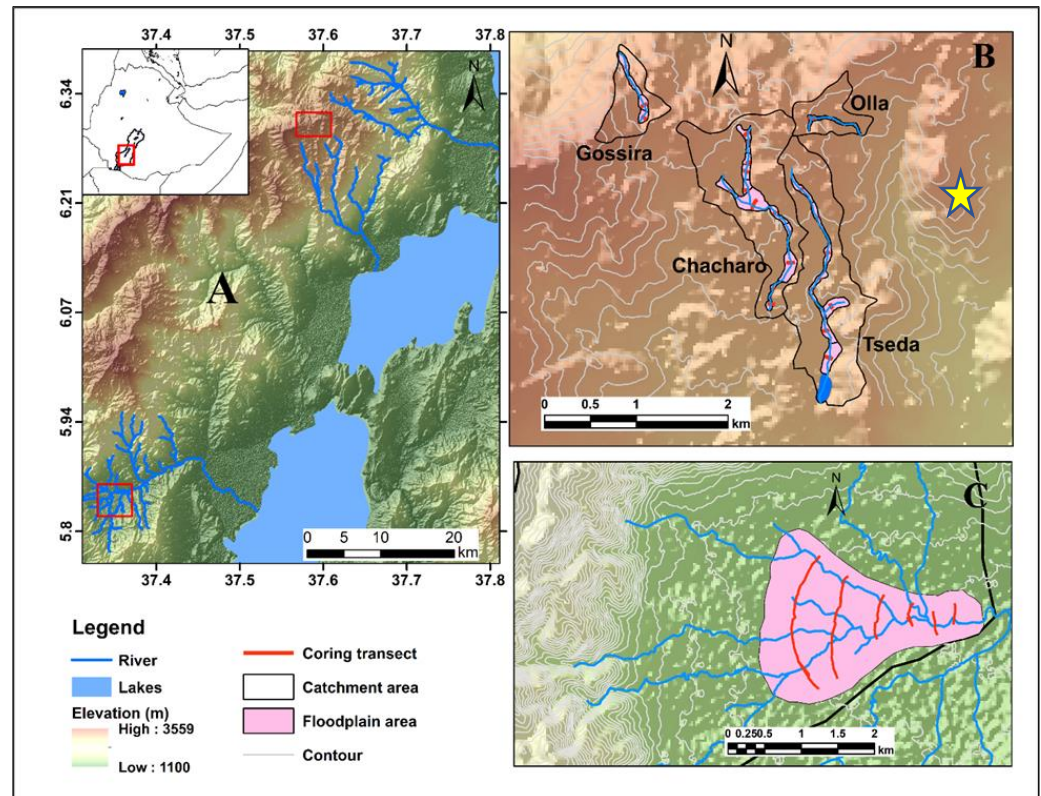


Figure 1. (A) Generalized topographic map of the Gamo highlands with indication of the Chencha and Dembelle floodplain sites, (B) Detailed map of the Chencha and (C) Dembelle floodplains with indication of the coring transects. The star indicates the Cave site (archaeological site).

2.2. Sediment Storage

Floodplain sediment storage was quantified by combining information on floodplain sediment stratigraphy obtained through soil coring and GIS-based floodplain mapping following the approach described by [2].

Information on floodplain stratigraphy and sediment thickness was obtained through coring with an Edelman or gauge hand auger, depending on sediment type. For each core, sediment color and texture were determined in the field, the latter with the feeling method. Sediment was cored until the bedrock or a clear transition from floodplain sediment to weathered bedrock could be noticed. In total, 103 corings were made in the Dembelle floodplain and 170 corings in the Chencha floodplains. In order to extrapolate field coring data to obtain an estimate of floodplain sediment storage at the catchment scale, the spatial extent of the floodplain was delineated by combining field and satellite data. The floodplain was divided into 31 and 6 homogeneous zones based on morphometric units (i.e., slope, valley width and soil texture) for Chencha and Dembelle, respectively, for which it is assumed that the mean thickness of the floodplain sediment deposits can be represented by a coring cross-section (Figure 3).



Figure 2. Boundary of floodplain in both studies valley systems (shown on google earth) and pictures taken in the field showing some specific locations. The bottom left picture shows a cutbank of a river channel that is incising into former floodplain and lacustrine layered deposits, whilst the bottom right picture shows sediment coring in the Gossira floodplain within the Chencha region.

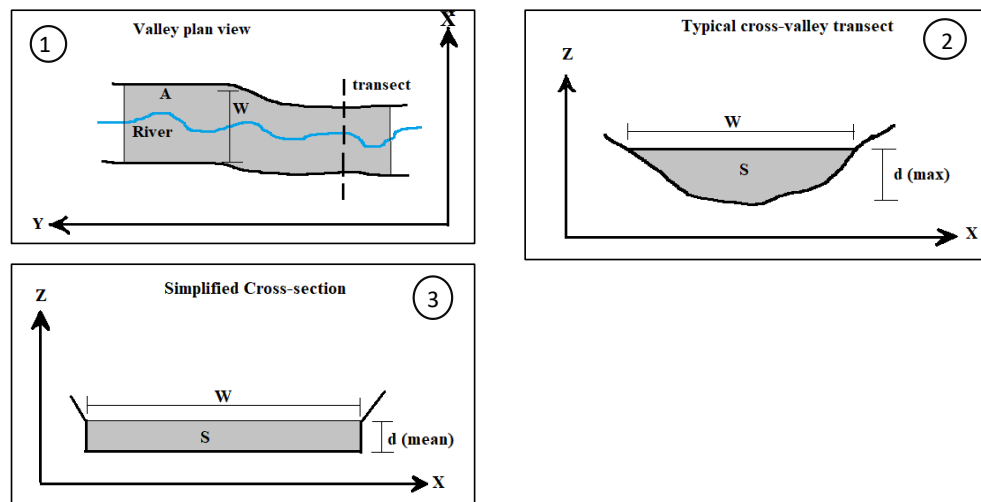


Figure 3. Method of floodplain sediment storage calculation. A is the area of the floodplain, W is the floodplain width, S is the area of sediment in a cross-valley transect and d (max) is the maximum thickness of the valley fill (modified after [2]).

$$V = A_i \times d_{\text{mean},i} \tag{1}$$

V—is the volume of sediment (m³)

A_i—is the area (m²) of the homogeneous floodplain unit i.

d_{mean,i}—is the mean depth (m) of sediment along the cross-section(s) representative for homogeneous floodplain unit i.

The sediment volume (m^3) is converted to a sediment mass (t) using the dry bulk density of the sediment (dBD, $t\ m^{-3}$), to allow a comparison with other sediment budget components, such as the sediment load of the river (t/year):

$$M_{\text{total}} = \sum_{i=1}^m V \times \text{dBD}_{\text{mean}} \quad (2)$$

The dry bulk density was obtained by sampling the floodplain sediment at 20 and 13 locations for Chenchu and Dembelle, respectively. All samples have a known volume (5 cm long sections from the gauge auger with a diameter of 3 cm) and were weighed after being oven-dried at 105 °C for 24 h.

The precision on the total sediment volume and masses were calculated using Gaussian error propagation as described by [2], including an error of 5% on the floodplain mapping and an error of 10 cm on the total sediment thickness as the transition between the floodplain sediments and the weathered bedrock or original soil was not always straightforward to delineate through coring.

2.3. Sediment Ages

Temporal changes in the fluvial response to environmental changes can be studied through the analysis of the age of the floodplain sediments and floodplain sedimentation rates [3,18]. Radiocarbon dating of organic matter retrieved from the floodplain sediments was performed on a total of 30 samples (22 samples for Chenchu and 8 samples for Dembelle). All radiocarbon dates were obtained at the Royal Institute for Cultural Heritage (RICHEL), Brussels, Belgium and were calibrated using the OxCal 4.4 software [25] and IntCal 20 calibration curve.

2.4. Cumulative Probability Functions of Sediment Ages

The temporal changes in geomorphic response to environmental changes can be studied through the analysis of cumulative probability functions (CPF). Several studies use the CPF of radiocarbon ages obtained from floodplain deposits for the analysis of a chronological database of fluvial activity and comparison of Holocene fluvial dynamics [5,6]. Refs. [6,26] showed that this technique results in a proxy of the fluvial system response to the external impacts, such as climate and land-use changes. Hence, CPF values were used in this study to understand the timing of the floodplain changes in the Chenchu and Dembelle catchments and to identify phases of increased floodplain activity. For data analysis, individual radiocarbon data were calibrated, and their distributions were summed to obtain a CPF. The shape of CPFs can be affected by a host of biases, such as sampling error and the shape of the calibration curves [27]. To overcome this bias, we divide the CPF of all radiocarbon data by a CPF of 100 equally spaced radiocarbon ages as is done in previous studies [5,26,28].

2.5. Sedimentation Rates

Based on the determined radiocarbon ages and depths of stored sediment, the actual sedimentation rates SR_a for a given time period are calculated for an individual pair of dated samples:

$$SR_{a,i} = \frac{D_i - D_{i-1}}{T_i - T_{i-1}} \quad (3)$$

where D_i and T_i are the coring depth and age of the corresponding dated samples (older sample) respectively and D_{i-1} and T_{i-1} are the depth and age of the above (younger stratigraphy) dated sample. T_i represents the mean value of the calibrated age. In the case of the uppermost dated sample $i = 1$ and $D_0 = 0$ and $T_0 = 0$. Because of the poor preservation of organic matter, few coring sites have multiple dates and a detailed analysis

of changing sedimentation rates through time with Equation (3) is not feasible. Hence, we also calculated mean sedimentation rates following [26,28]:

$$SR_{m,i} = \frac{(D_i)}{(T_i)} \quad (4)$$

This approach allows the comparison between cores with different sampling densities and hence minimizes the effect of coring densities in calculated sedimentation rates between individual cores. When the database is sufficiently large, the analysis of mean sedimentation rates for different time periods allows to obtain an overall indication of the changing sedimentation rates through time for a given region. Moreover, the use of a mean, time-integrated, sedimentation rate (SR_m) allows for the application of a simple modeling approach, that enables to calculate the actual sedimentation rate through time [5,29]. Hence, in this study, the modeling approach was applied to estimate (SR_m) at each point in time based on SR_a per period of 100 years over the last 10,000 years. A Monte Carlo approach was employed to study trends in floodplain sedimentation rates over the last 10,000 years. Different periods of increase and decrease in floodplain sedimentation rate were simulated to determine the modeled mean sedimentation rate that best fits the observed ones. In total, approximately 8160 model runs over the range of 0.06 to 20 mm, a^{-1} were evaluated using the model efficiency (ME) and root mean square errors (RMSE).

$$ME = 1 - \frac{\sum_{i=1}^n (O_i - P_i)^2}{\sum_{i=1}^n (O_i - O_{mean})^2} \quad (5)$$

$$RMSE = \sqrt{\frac{\sum_{i=1}^n (P_i - O_i)^2}{N}} \quad (6)$$

where O_i is the observed SR_m value (individual radiocarbon dated SR_m , P_i model predicted SR_m value for each observation, O_{mean} mean of all observed SR_m and N is number of observations.

It should be stressed that the sedimentation rates calculated with Equations (3) and (4) are in fact net sedimentation rates, i.e., these provide an estimate of the rate at which the present-day sediment record has been accumulating.

2.6. Sediment Mass Accumulation

In order to obtain floodplain sediment mass accumulation rates, soil depths were converted to mass of accumulated sediments based on the following equation.

$$M_{layer,i} = d_{layer,i} \times dBD \quad (7)$$

with $M_{layer,i}$ the sediment mass per unit floodplain area of dated sediment unit i ($t m^{-2}$), $d_{layer,i}$ thickness of dated sediment unit i (m) and dBD the dry bulk density of the sediment ($t m^{-3}$). Additionally, the mass of coring ($M_{coring,i}$) per unit floodplain area was also calculated for each coring depth, $d_{coring,i}$ (unit coring depth per unit floodplain area, m) to determine the relative mass accumulation ($M_{Relative,\%}$) after the deposition of the dated sample.

$$M_{coring,i} = d_{coring,i} \times dBD \quad (8)$$

$$M_{Relative,\%} = \frac{M_{layer}}{M_{coring}} \quad (9)$$

Relative floodplain mass accumulation was plotted versus age for the different dated coring transect to understand the sedimentation history. Basically, relative floodplain accumulation means the proportion of sediment mass per unit floodplain area deposited at the moment of deposition compared to the total sediment accumulation for the considered coring [18]. In general, relative accumulation amount is important to make straightforward

comparison of corings with different total long-time (Holocene) sediment accumulation. Whilst the valley size influences the relative sediment mass accumulation, the mean value of sediment mass accumulated in the entire catchment was calculated by taking into account the weight according to the size of the catchments [29].

3. Results

3.1. Floodplain Sediment Stratigraphy

3.1.1. Chencha Sediment Stratigraphy

The Chencha floodplain is filled with sediment that reach a depth of 4 to 5.20 m. Figure 4a indicates the detail of floodplain sediment stratigraphy for one coring location in the Chencha catchment. Details of the other profiles can be found in the Appendix B (Figure A1). The dominant sediment soil texture recovered along each transect consist of fine-grained sediments (mainly clay, silty clay and clay loam), sandy sediments (sandy loam, loamy sand, and sandy clay loam) and medium-grained sediments (loam and silty loam). The transitions between these units are, however, often very smooth and often difficult to observe in the field. The field-based observations of the sediment stratigraphy does suggest that at the long-term, sedimentation was more or less continuous, i.e., without clear signs of erosional hiatus. Below the fine-grained sediments, a heterogenous mixture of clay, sand and angular gravel fragments can be found, which is interpreted as the transition to the weathered bedrock. For the sediment storage calculations, all units above the latter sediment unit are considered as floodplain sediment although no clear distinction can be made between alluvial and colluvial valley deposits.

3.1.2. Dembelle Sediment Stratigraphy

The Dembelle floodplain sediment storage is comparatively much thicker and can reach a depth of 7 to 8 m (Figure 4b). In this floodplain, sandy and clay textured sediments are dominating particularly in the middle and upper part of the floodplain. Figure 4b shows a detail of the sediment stratigraphy in the Dembelle floodplain along the first transect. The sediment units in this floodplain are quite complex as the floodplain is located next to the steep mountain slope in the upstream part of the floodplain. Though the heterogeneity is dominating between the units in the upstream areas, the transition from one unit to the other is very abrupt contrary to what was observed in Chencha. As with Chencha, below the fine-grained sediments, medium gravel to small angular gravel fragments size can be found, which considered as the transition to the parental material or weathered bedrock. Looking at the stratigraphic record obtained from the sediment corings, complemented with field observations of the river cutbank incised into the sediments (Figure 2) and the overall shape of the sediment deposit, we believe that the Dembelle floodplain is in fact a former depression, potentially of tectonic origin, that first has been infilled by a combination of lacustrine (fine-grained) and fluvial (coarse-grained) sediments.

3.2. Sediment Volumes and Masses

The quantified floodplain sediment storage for each sub-catchment of Chencha and Dembelle is summarized in Table 1. A total volume of sediment in the order of $1.09 \pm 0.14 \text{ Mm}^3$ and $13.66 \pm 0.43 \text{ M m}^3$ are stored within the headwaters of Chencha and Dembelle catchments, respectively. This corresponds to sedimentation rate of $\sim 3.22 \pm 0.33 \text{ kt ha}^{-1}$ catchment area in Chencha, whereas it is $\sim 3.76 \pm 0.22 \text{ kt ha}^{-1}$ catchment area in Dembelle floodplain. There is a large variation in the average thickness of the floodplain deposits between the different sub-catchments and coring sites. Whilst floodplain gradient suddenly increases, both sediment masses and volume were decreasing remarkably (Figures 5 and 6). In all sub-catchments, the largest deposition is found in the upper part and gradually decrease downstream along the river course except along the Tseda floodplain where the upstream part of the floodplain is characterized by very steep slope (Figure 6).

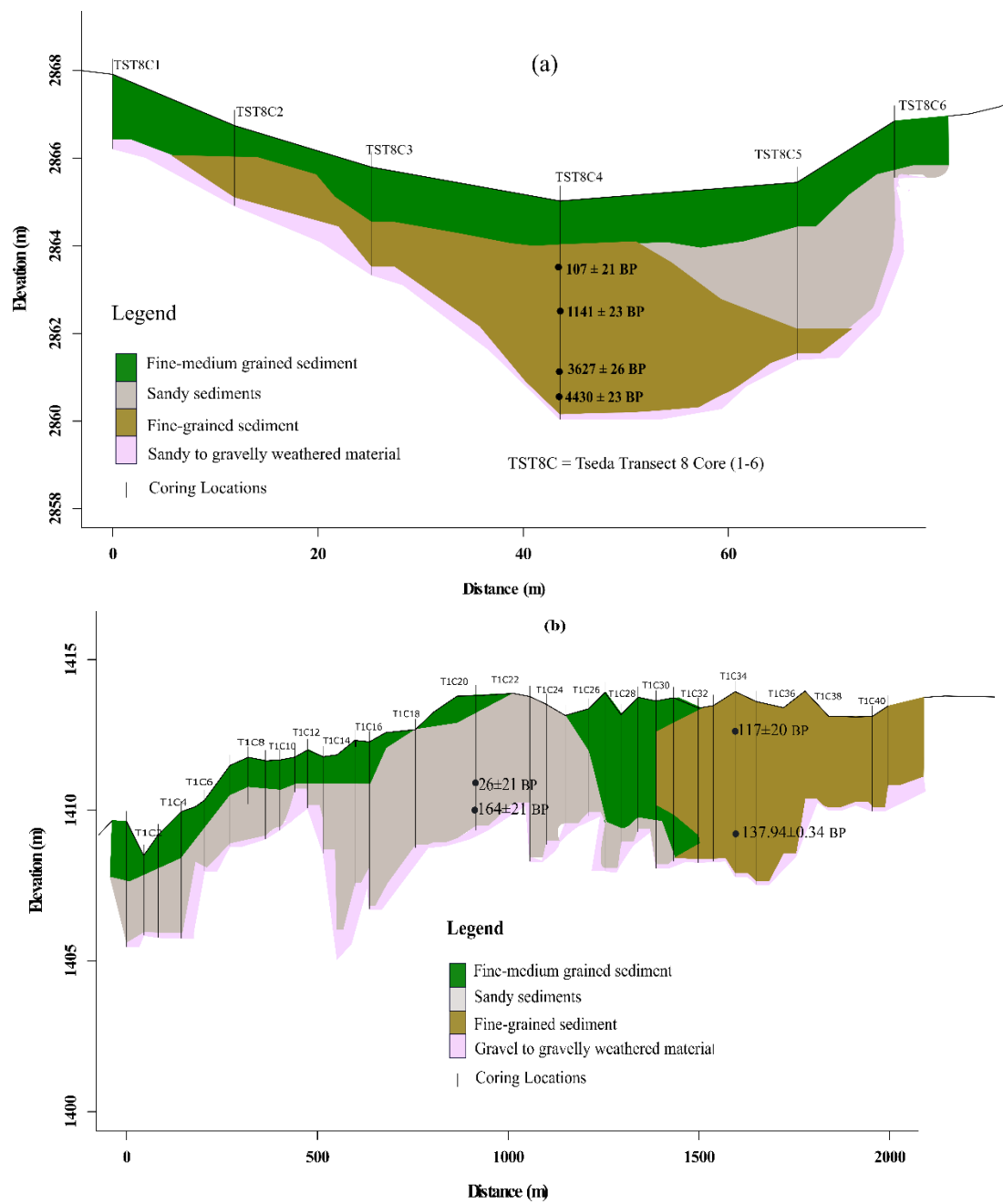


Figure 4. Example a typical cross-section with indication of the various sedimentary units in the (a) Chench and (b) Dembelle catchment. Radiocarbon ages are reported in non-calibrated years BP.

Table 1. Overview of the floodplain area and sediment deposition within different sub-catchments.

Location	Sub-Catchment	Catchment Area (ha)	Floodplain Area (ha)	Sediment Volume (M m ⁻³)	Sediment Mass (Mt)	Floodplain Sediment Storage per Unit Catchment Area (kt/ha)
Chench	Chacharo	151	22	0.49 ± 0.03	0.59 ± 0.07	3.95 ± 0.48
	Tseda	155	17	0.41 ± 0.03	0.49 ± 0.06	3.19 ± 0.38
	Olla	32	3	0.04 ± 0.01	0.05 ± 0.01	1.71 ± 0.39
	Gossira	40	6	0.13 ± 0.01	0.16 ± 0.02	4.03 ± 0.48
	Total	379	47	1.09 ± 0.14	1.31 ± 0.10	3.22 ± 0.33
Dembelle	Dembelle	4953	400	13.66 ± 0.43	18.61 ± 1.11	3.76 ± 0.22

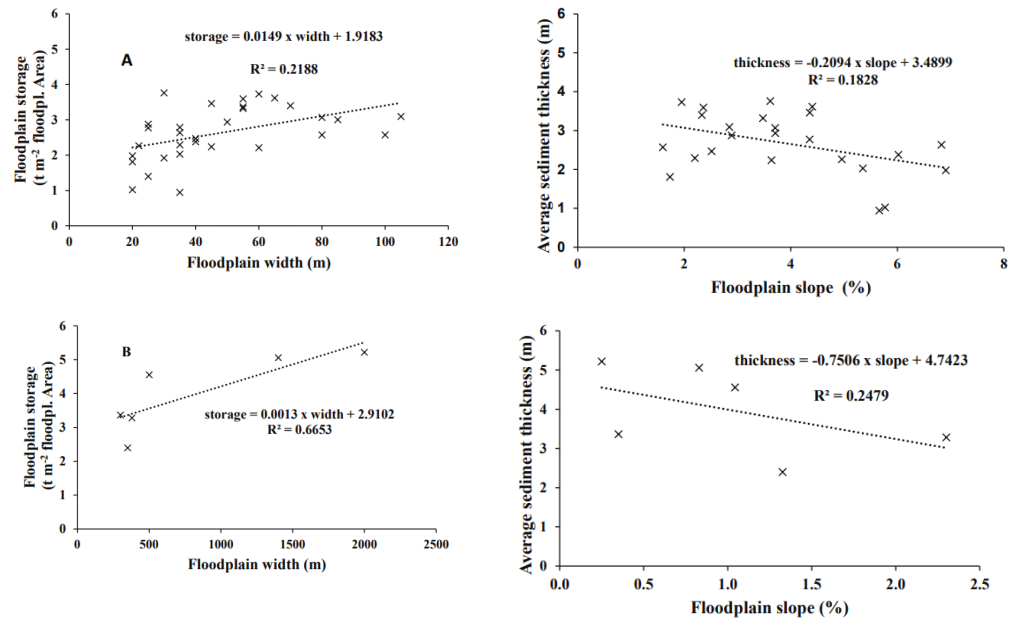


Figure 5. Relations of floodplain storage and mean sediment thickness in function of floodplain width and slope for Chencha (A) and Dembelle (B).

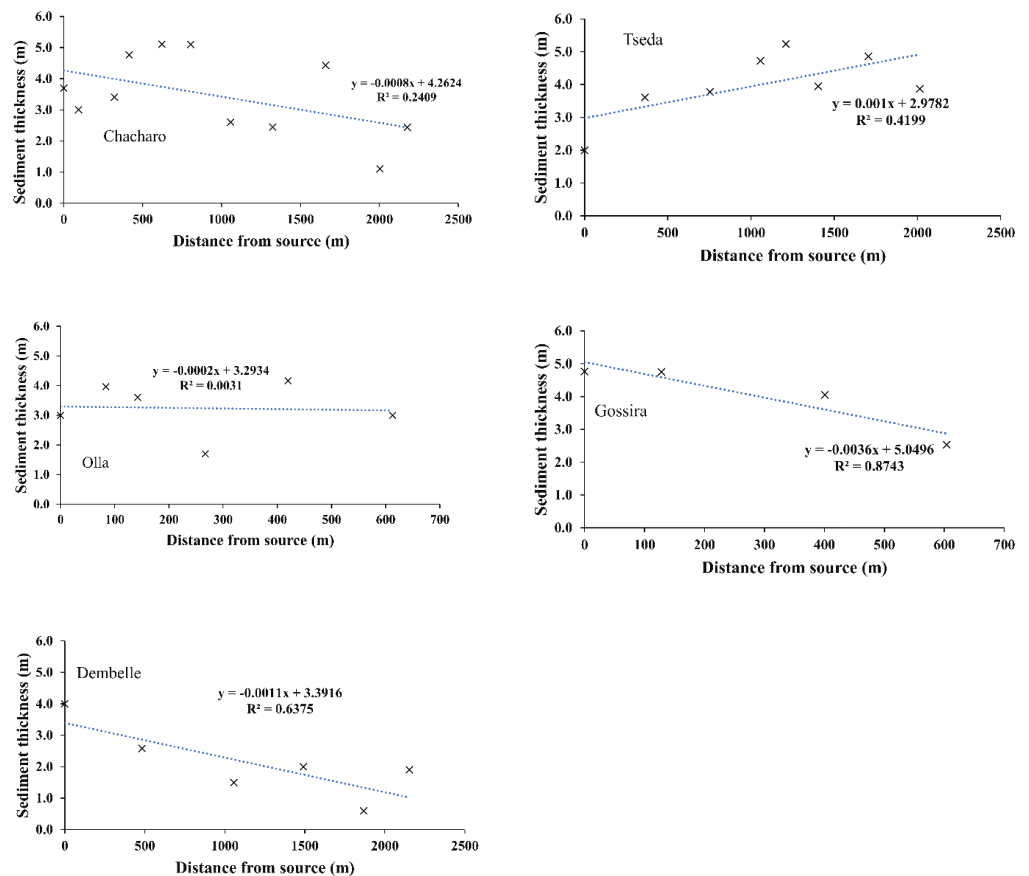


Figure 6. Average floodplain sediment thickness in relation to distance from the source of the river.

3.3. Dating Results

In total, 8 bulk samples from the Chencha floodplain and 22 wood and charcoal samples from both Chencha and Dembelle at different depths were dated (Table A1). The calibrated radiocarbon age of sampled datable materials range between 43,706 BC

to 1923 AD in Chencha floodplain, whereas all samples from the Dembelle floodplain are very young and range between 1665 to 1923 AD (Table 2). Only at three sites, pre-Holocene ages were obtained, all at the bottom of the sediment core in the sandy to gravelly weathered layer.

Table 2. Model efficiency for the best performing scenario of sedimentation increase based on radiocarbon ages of the Dembelle floodplain.

Scenario: Increase from	ME	RMSE
1800 AD (with a 13 mm a ⁻¹ increasing to present)	0.340	1.34
1900 AD (with a 17 mm a ⁻¹ increasing to present)	0.339	1.35

3.4. Cumulative Probability Function

A CPF plot of all Holocene radiocarbon ages obtained from the sediment record is shown on Figure 7. The results of the probability density analysis suggest a rather stable fluvial system during the early Holocene and increased geomorphic activity during the Middle and Late Holocene. The CPF shows major a first sign of fluvial activity in the studied floodplains at approximately 6000 to 6500 cal BP and some localized activities in the period 6500–3500 cal BP. An abrupt rise, and continuity, in fluvial activity can be observed from approximately 2000–1600 cal BP onwards in the Chencha floodplains. In the Dembelle region, however, periods of active sedimentation are more restricted to the last 400 years and no sediment ages prior to this period could be identified.

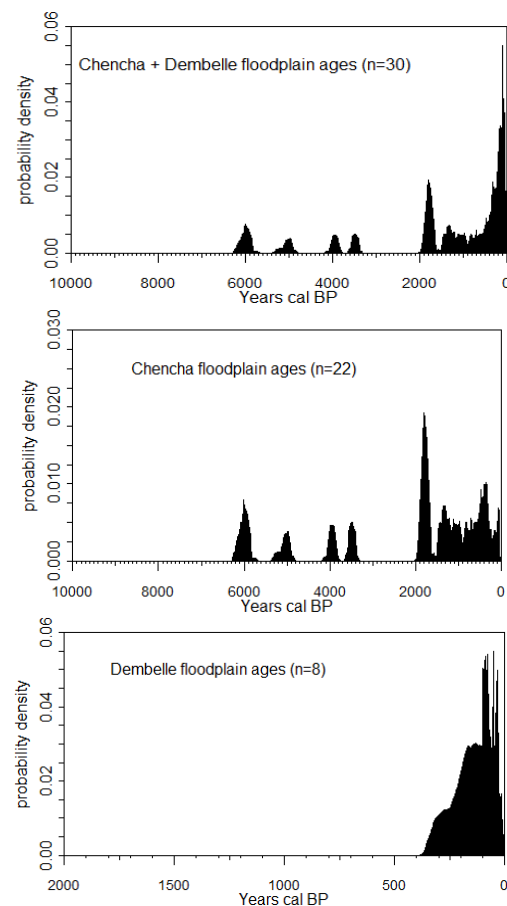


Figure 7. CPF of radiocarbon ages of the datable materials for Chencha and Dembelle floodplains. Probability was divided by the probability of 100 equally spaced ages and corrected for the biases.

3.5. Floodplain Sedimentation Rates

Figure 8 shows the age-depth models for corings for which we have multiple dates (i.e., within the Gossira, Olla and Tseda sub-catchments of Chenchu) in one core. Figure 9 shows the mean sedimentation rates for both sites. The age-depth models (Figure 8), as well as the visual inspections of the sediment stratigraphy do not show major hiatus in sedimentation and thus the net sedimentation rates shown here can be considered to be representative of the long-term mean sedimentation rate. The mean sedimentation rates are very low prior to 4000 cal BP, whereas it shows a strong increase after 3000 cal BP in the Chenchu floodplains. Sedimentation rates peak at approximately 2000 cal BP and a clear decline can be seen after 1000 cal BP. The Dembelle floodplain sedimentation is very young as it started approximately from 400 cal BP with a peak value obtained 165 cal BP. The mean sedimentation rate, however, provides an average over sometimes very long time periods, and thus do not provide a good insight in the actual sedimentation rates at a given time period. Different scenarios for the evolution in actual SR were therefore simulated and used to calculate mean SR which were compared with the observed record shown in Figure 10.

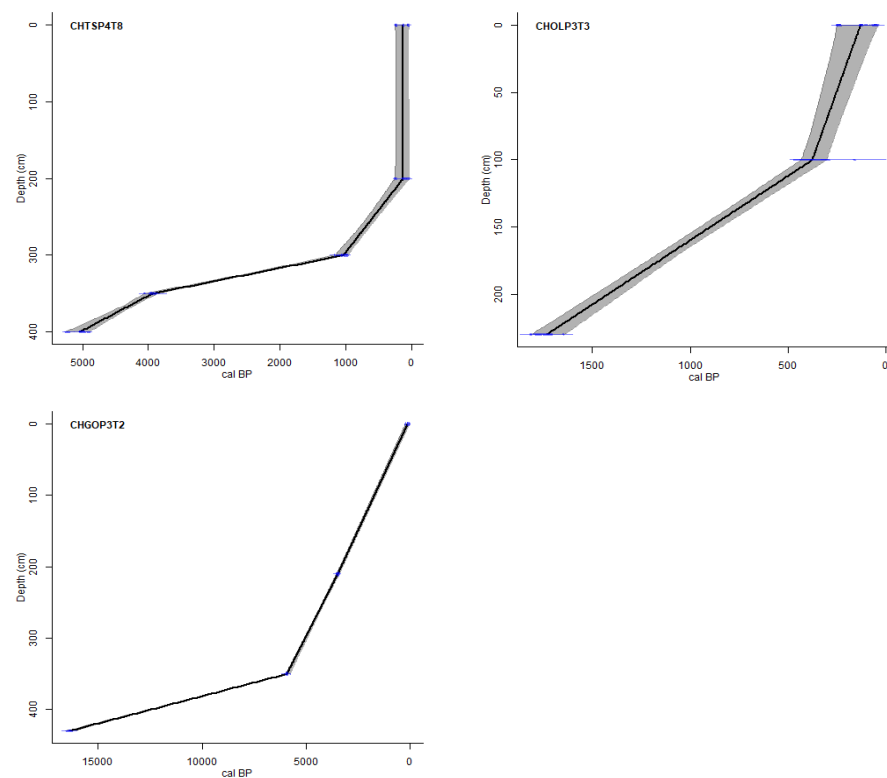


Figure 8. Overview of the coring data based on the sampling depths and radiocarbon ages relations or actual sedimentation rates for selected coring. The blue horizontal lines indicate the sampled and dated depth with 95% probability density, whereas the black line indicates sedimentation history.

Model efficiency values for several sedimentation rate scenarios were performed to determine the best sedimentation trend (Figure 11 and Table 3). The Monte Carlo modeling approach shows that the scenario with an early increase in sedimentation rate (with 20 mm a^{-1} increase) in approximately 200 AD, and this for a duration of 1000–1200 years, best fit to the field data Figures 10A and 12. Next, sedimentation decreased again and a second rise in sedimentation at approximately 1800–1900 AD again best fit the observed radiocarbon ages. These scenarios have the highest ME and lowest RMSE values. It is clear from Figure 11 that the model is especially sensitive to the start of the first increase in sedimentation, and lesser to the renewed start of sedimentation or the exact height of the sedimentation rate. Additionally, the duration of the first phase of increased sedimentation

most likely varied between 600 and 1600 years as the majority of model runs with a high ME have such a duration (Figure 12).

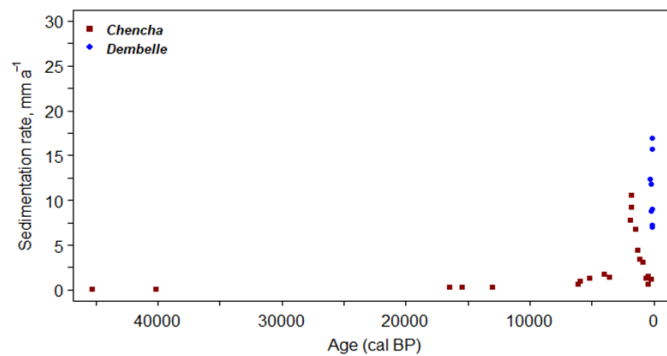


Figure 9. Changing mean floodplain sedimentation rates in Chencha and Dembelle from 46,000 to 0 cal BP based on 30 radiocarbon data.

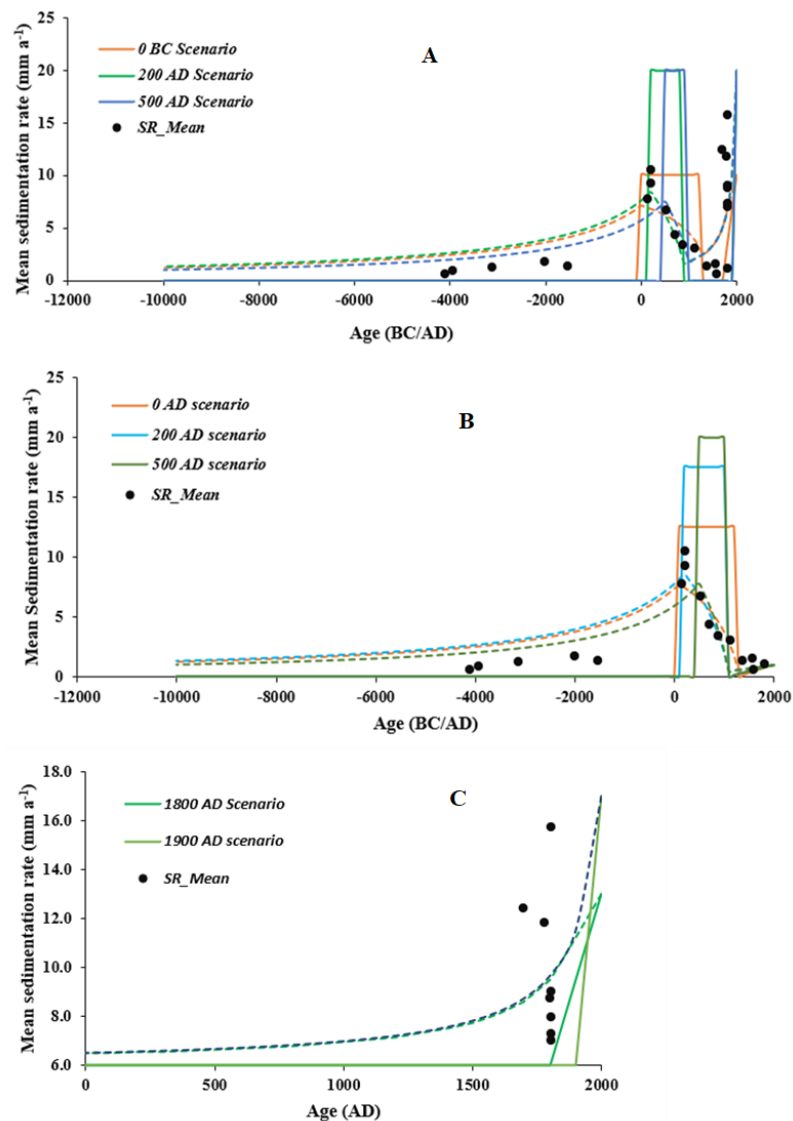


Figure 10. Mean sedimentation rate (black dots) of (A) both Chencha and Dembelle, (B) Chencha and (C) Dembelle, and model results from the mean sedimentation rates SR_m modeling approach over the Holocene period. The lines represent the alternative scenarios in the onset of increased and decreased sedimentation rate trends.

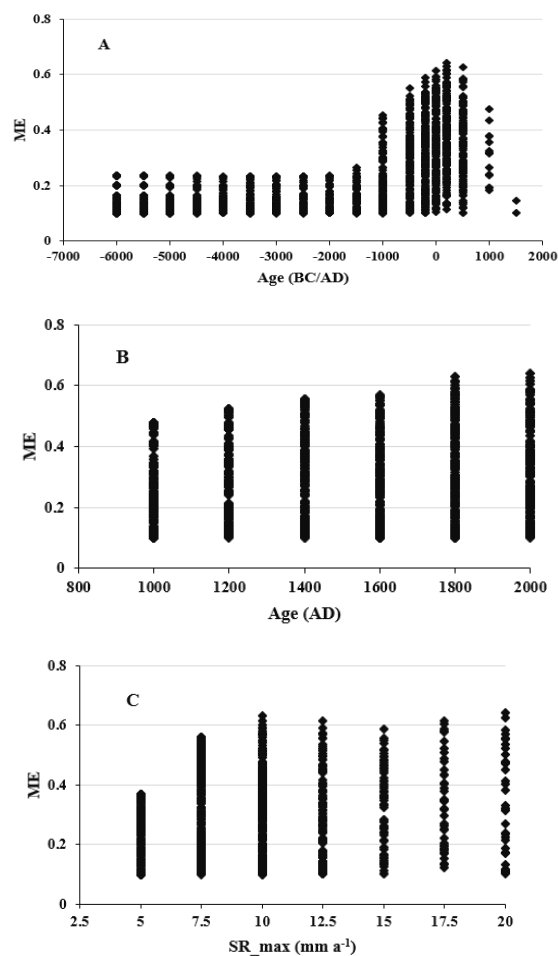


Figure 11. Model efficiency for several scenarios as a function of the (A) start of first sedimentation rate (SR) increase, (B) start of second SR increase and (C) height of the SR both for Chencha and Dembelle floodplain.

Table 3. Model efficiency for a selection of the best performing scenarios of sedimentation increase based on radiocarbon ages of the Chencha floodplain.

Scenario: Increase from	ME	RMSE
0 BC (with a 12.5 mm a ⁻¹ increasing for 1800 years)	0.76	1.34
200 AD (with a 17.5 mm a ⁻¹ increasing for 1000 years)	0.81	1.18
500 AD (with a 20 mm a ⁻¹ increasing for 600 years)	0.74	1.39
1800 AD (with a 2.5 mm a ⁻¹ s increasing to present)	0.78	1.28

Furthermore, since it is clear from the observational record that a large discrepancy in sediment ages were obtained for the Chencha and Dembelle regions, separate model runs and model efficiency values for each region were obtained to establish the best performing sedimentation trend. Figures 10B, 13 and 14, and Table 3 shows the main results for the Chencha floodplain, whereas the results for Dembelle are shown in Figures 10C and 15 and Table 3. The model approach shows that the scenario with an increase in sedimentation rate of 1000–1200-year duration (with constant increasing in sedimentation rate at 17.5 mm a⁻¹) in approximately 200 AD fit best to the mean sedimentation rate observed in the Chencha floodplain (Figures 13 and 14). In the Dembelle floodplain, the scenario with a first increase in sedimentation in approximately 1800 AD fit best to the observed mean data (Figures 10C and 15).

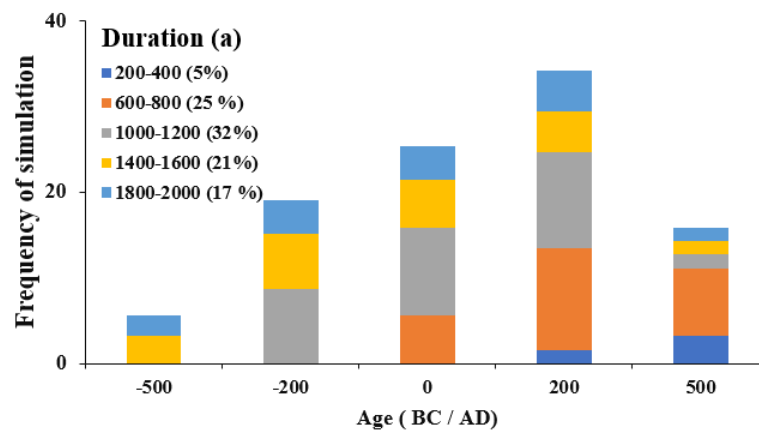


Figure 12. Histograms of the 5% best performing sedimentation models (n = 408) based on the ME (model efficiency) for floodplain sedimentation of Chencha and Dembelle. While the bars are centered at the period assumed for the start of increased sedimentation, the fill is chosen according to the assumed duration of the period with increased levels of sedimentation.

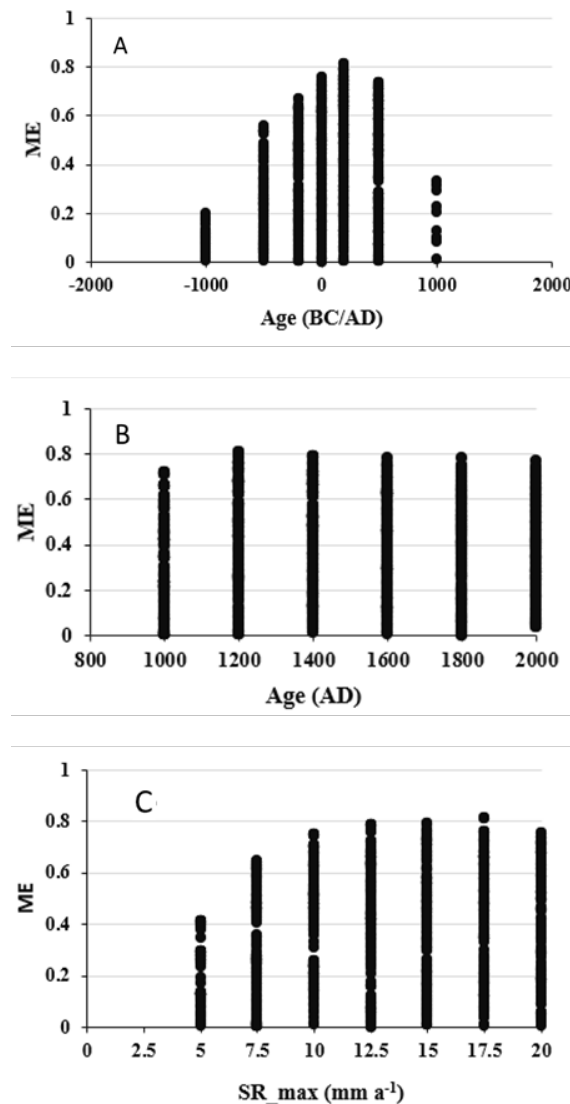


Figure 13. Model efficiency for several scenarios as a function of the (A) start of first sedimentation rate (SR) increase, (B) start of SR decrease and (C) height of the SR for Chencha floodplain.

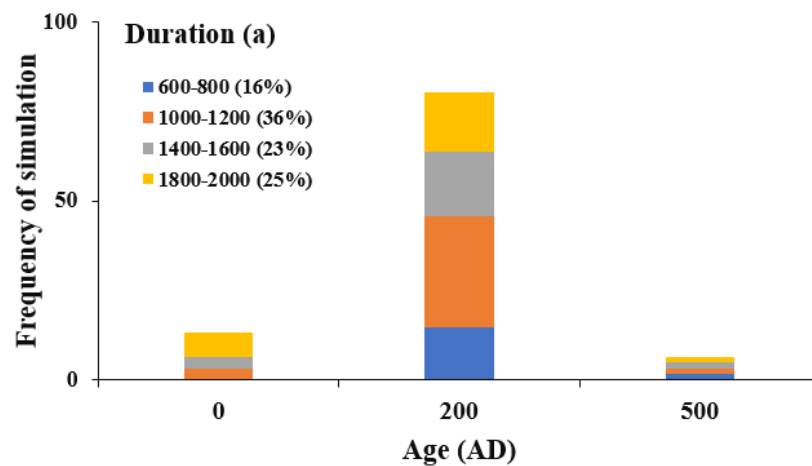


Figure 14. Histograms of the 4% best mean of sedimentation models (n = 326) based on the ME for floodplain sedimentation of Chencha.

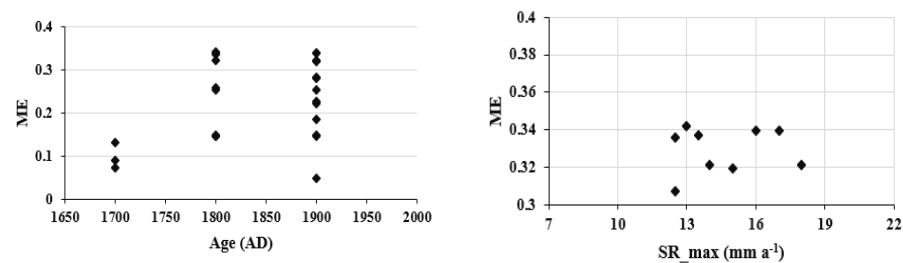


Figure 15. Model efficiency for several scenarios as a function of the start of first sedimentation rate (SR) increase, and height of the SR for Dembelle floodplain.

3.6. Sediment Mass Accumulation

Figure 16 shows the relative sediment mass accumulation for the Chencha region, which provides a summary of catchment-wide sedimentation patterns. In all floodplains sediment storage increased strongly after 1 AD. On average, 70% of all the stored sediment in the studied floodplains in the Chencha area is deposited in the last 2000 years. For individual valley systems, this varies between 54 and 82%. For the Dembelle area, on average, 80 % of all sediment stored is deposited in the last 200 years (Figure 17).

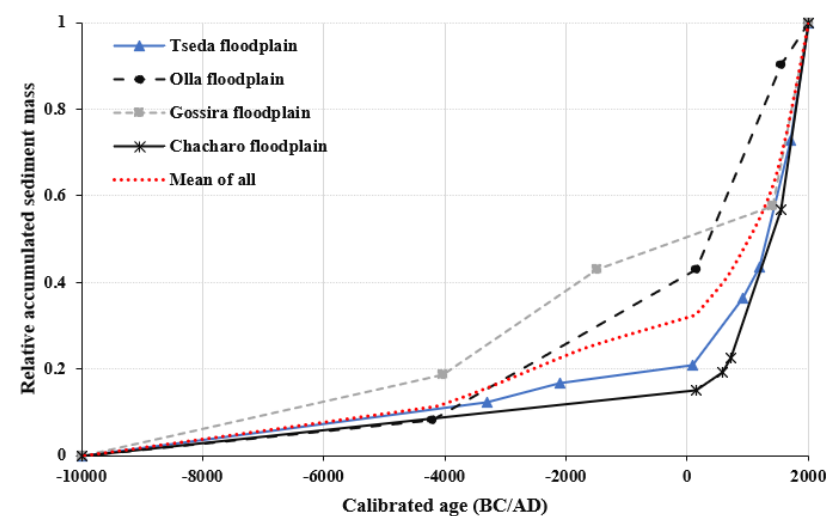


Figure 16. Age and average relative accumulated sediment mass for the different dated corings in floodplain deposits in the Chencha catchments (broken line in red color is the mean value for the entire catchment).

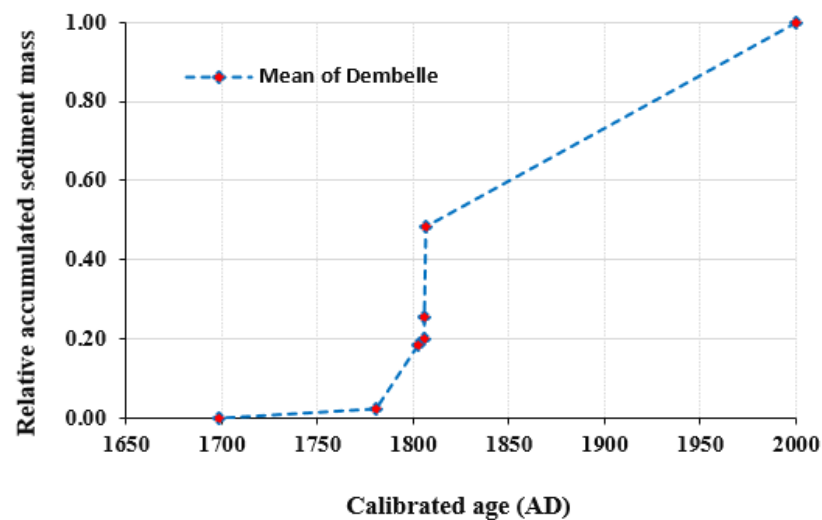


Figure 17. Age and average relative accumulated sediment mass for the different corings in the Dembelle floodplain deposits.

4. Discussion

For the first-time, long-term floodplain sediment storage within the two upland catchments in the Gamo highlands of the Ethiopian Rift Valley was quantified, and the timeframe of deposition established. Although, limited available datable organic material could be retrieved from the floodplain deposits, it was possible to identify periods during which the floodplains have actively stored sediment. The construction of CPF based on radiocarbon ages indeed provides a detailed picture of phases during which erosion and sediment deposition was important. The CPF show dominant peaks of geomorphic activities after the period of ca. 2000 cal BP compared to those for the periods between ca. 46,000–3000 cal BP (Figure 6). Since at two sites material of approx. 40–46 ka cal BP could be observed, and at another site material of ca. 13 ka cal BP in the clayey unit with angular gravel directly below the fine-grained sediments of middle to late Holocene age, suggests that the landscape was relatively stable for quite some time. We interpret the clayey unit with angular gravel as the weathering palaeosols on top of the bedrock or a saprolite on the bedrock as described by [24] in the Gamo highlands. This surface shows no net changes in elevation since at least ca. 46 ka cal BP. The fine-grained sediment above this layer is interpreted as the result of topsoil erosion in the catchment where fine earth material is deposited as colluvial and alluvial sediment. Our results show that this product of hillslope erosion starts at an individual location between ca. 6000 and 3600 cal BP, but becomes more widespread from ca. 2000 cal BP. These results are in agreement with the findings of [24] who dates the colluvial layer on top of the palaeosols at an age of 920–810 cal BC.

The result of CPF analysis generally suggests a tendency toward a stable fluvial system during the early Holocene and increased geomorphic activity during the Middle and Late Holocene. Several studies have related the geomorphic dynamic to driving forces, such as climate change and human-induced environmental changes in different part of the world. For instance, ref. [16] has reported that the peak fluvial sediment dynamics observed in central Tunisia has a good match with the flooding occurred during the Mid-Holocene period based on the constructed CPF of radiocarbon ages. Likewise, other studies in the temperate and Mediterranean region based on the CPF of radiocarbon ages have also reported that the fluvial sediment dynamics coincided with the period of paleoclimate change and increased anthropogenic activity during the Holocene in the region [6,7,20,26]. Some archaeological evidence from different caves within the Gamo highlands along with their radiocarbon ages indicates that human activities emerged since ca. 6500 cal BP [23]. This is nearly the same period during which the sedimentation starts according to the CPF curves. Furthermore, archaeological evidence has also uncovered that agricultural activity could have been introduced in this region during the second millennium BP, based on the

sample of single wheat seed retrieved from the site. It is apparent from Figure 18 that most of the CPF of human related artefact material ages shows dominant peak at approximately ca 1700 Cal BP. A study by [30] has provided the evidence that stonewalled indigenous terraces have long been a part of agricultural activities in the region and were built and used over the last 800 years (based on radiocarbon dating), particularly in Chench. This indicates that it has been a long time since agricultural activity was introduced in the region. Thus, 1700 cal BP is assumed to be the period when human related activity was ultimately started in the region. This period is roughly corresponding to the first significant increase in sedimentation rates as was modeled for Chench region, suggesting that sediment dynamics in the Gamo highlands are largely controlled by human impact. Furthermore, the presence of agricultural terraces dated at 8000 years also shows that early erosion control measurements have been taken following the first major peak in soil erosion in the Chench area. This might explain the decline in sedimentation rate. Apart from human impact, short-term climate variability may also have played a secondary role.

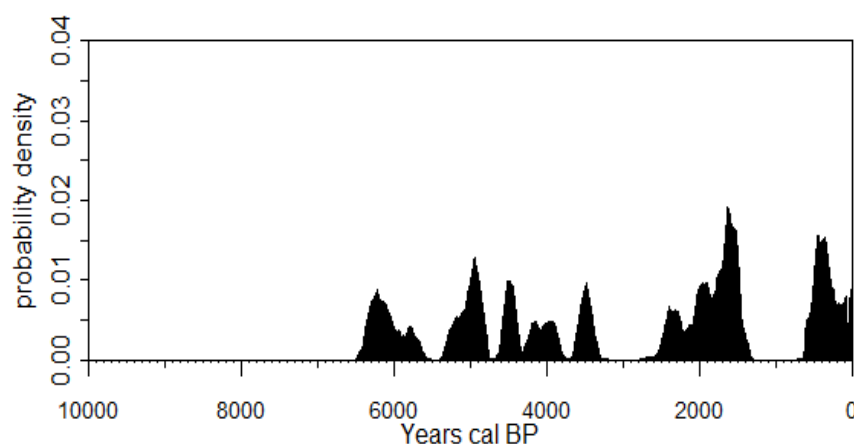


Figure 18. Radiocarbon dates from the Boreda Gamo Cave archeological sites (approximately 13 km distant from the Chench study site at an elevation above 2500 m) based on artefact materials [23].

Some studies in the rift valley lake basins have reported that there has been a short-time alteration in the climatic condition particularly during the Mid-Late Holocene period [31]. The detailed lake sediment record of the rift valley lakes system indicates the wetter condition at approximately ca. 2400 to 1350 cal BP. This resulted in the rise of rift valley lakes level between ca. 1900 to 1400 cal BP, which could be related to elevated precipitation during this period [31]. Investigation of East Africa's paleo-environmental change by [32] also indicate that the period from 4000 to 1000 BP was the warm and dry punctuated by episodes of heavy convective precipitation. Similarly, ref. [33] confirmed that the period from ca. 3023 to 1670 cal BP represents a progression from cool dry to wet condition based on a peat deposit from the Kapsabet swamp in western Kenya. Thus, a landscape that is more and more inhabited and impacted by humans, leading to less vegetation cover, in combination with a shift to a wetter climate, may have been the ideal setting for the first erosion wave. The second erosion and sedimentation peak which could be observed for both Chench and Dembelle is much more recent and corresponds to the growing population numbers in the last two centuries and the erosion crisis observed in many parts of the Ethiopian Highlands [34–36]. It is striking to note that only in the highest part of the landscape, i.e., on the highland plateaus near Chench, earliest human impact can be detected, whereas further downslope near Dembelle, landscape changes are much more recent. It is hypothesized that original inhabitation of the region is restricted to the higher elevations and that only with increasing population levels, people are migrating downslope and degrading the steeper parts of the landscape.

It was obtained that the floodplain sediment storage is highly variable among the catchments, with an average value of 3.22 ± 0.33 and 3.76 ± 0.22 kt ha⁻¹ catchment area in Chench and Dembelle floodplains, respectively. Although we do not have a well-

established regional database that demonstrates the sediment storage in the floodplain and its variability in the region, our result is in the same order of magnitude with other findings from the same catchment sizes in other part of the world [2,4,5]. For instance, ref. [2] reported a floodplain sediment deposition value of $2.65 \pm 1.18 \text{ kt ha}^{-1}$ catchment area in the Nethen River floodplain, which is a small tributary of the Dijle river of Belgium. Similarly, ref. [5] reported that sediment deposition masses ranges between 2.41 ± 0.18 and $13.60 \pm 0.61 \text{ kt ha}^{-1}$ floodplain area within different tributaries of the 800 km² large Dijle river catchment in the European Loess Belt. Floodplain sediment storage over a long timescale is the integration result of several factors, such as the linkage between hillslope sediment delivery and floodplain properties [4]. In this study, we noticed that the floodplain sediment storage has a significant relationship with some floodplain properties. The variability in sediment storage could be explained by the differences in the floodplain forms, varying width of the floodplain in different valley sections and different valley gradients (Figure 5). Comparably, the Dembelle floodplain has a higher deposition amount than Chench, which could be related to most probably a rapid infill of a lake environment within a tectonic depression, and rapid deforestation in the recent periods at lower elevation. At present, the Dembelle depression is being incised again and turned into a net sediment source due to the intensive regressive erosion of a tributary of the Elgo river (Figure 2).

5. Conclusions

In this study, for the first-time, the long-term floodplain sediment storage and sedimentation dynamics of rivers in the Southern Ethiopia Rift Valley is presented. The results demonstrate that floodplain sediment storage predominantly dates from the last 2000 years, with approximately 70% of the total sediment mass accumulated in this period. The available datable organic material in the floodplain sediment has enabled us to get a catchment wide insight in the past sediment dynamics. The CPF of radiocarbon dating ages shows dominant peaks starting from ca. 2000 cal BP on up to ca 1600 Cal BP, whereas the lowest probability peak in the last 2000 years is observed between ca 1600 and 1500 Cal BP. Based on the archaeological evidence and different related studies in the region, the influence of anthropogenic land use on the studied sedimentary archives could be identified. Whilst human impact made the landscape more vulnerable to soil erosion in the last 2000 years, a change toward a wetter climate, as observed by lake level fluctuations at approximately 1900 to 1400 Cal BP, may have further triggered the first erosion and sedimentation wave in the Gamo Highlands.

Author Contributions: A.K.T. carried out data collection, data analysis, and writing—original draft preparation. G.V. participated in conceptualization, methodology, writing—review and editing, and supervision. M.C. participated in conceptualization, methodology, writing—review and editing, and supervision. G.G. participated in conceptualization, methodology, writing—review and editing, and supervision. F.A. participated in data collection and analysis, and review and editing. W.S. participated in data collection and analysis, review, and editing. All authors have read and agreed to the published version of the manuscript.

Funding: This research was funded by VLIR-UOS in the framework of the Inter-University Cooperation with Arba Minch University. Project no. AMU ET2017IUC035A101.

Data Availability Statement: Not applicable.

Acknowledgments: We would like to acknowledge VLIR-UOS for financial support. We thank VLIR-Arba Minch-IUC office team, KU Leuven, Arba Minch University, and all other individuals who participated in field data collection and processing.

Conflicts of Interest: The authors declare no conflict of interest.

Appendix A

Table A1. Radiocarbon age for organic matter retrieved from the Chencha and Dembelle floodplain sediments.

Sample ID	Lab Code	Location	Depth (m)	Material	Conventional Age (14 C a BP)	Calibrated 14 C age ($\pm 2\sigma$)
CHCHP2T1D350	RICH-30112	Chencha	3.5	Wood	1521 \pm 25	438–605 AD
CHCHP2T5D300	RICH-30554	Chencha	3.0	Charcoal	34,897 \pm 168	38,571–37,681 BC
CHCHP2T8D310	RICH-30104	Chencha	3.1	Charcoal	1320 \pm 22	655–775 AD
CHCHP3T4D400	RICH-30127	Chencha	4.0	Bulk sample	12,843 \pm 34	13,581–13,251 BC
CHCHP4T11D240	RICH-30128	Chencha	2.4	Wood	314 \pm 21	1498–1644 AD
CHCHP4T6D260	RICH-30103	Chencha	2.6	Charcoal	42,758 \pm 131	43,706–42,866 BC
CHCHP5T2D200	RICH-30286	Chencha	2.0	Wood	1841 \pm 28	123–310 AD
CHGOP2T3D180	RICH-30133	Chencha	1.8	Charcoal	562 \pm 21	1322–1422 AD
CHGOP3T2D210	RICH-30135	Chencha	2.1	Bulk sample	3263 \pm 24	1612–1454 BC
CHGOP3T2D350	RICH-30342	Chencha	3.5	Bulk sample	5162 \pm 28	4045–3818 BC
CHGOP3T2D430	RICH-30287	Chencha	4.3	Charcoal	13,560 \pm 45	14,595–14,261 BC
CHGOP4T1D110	RICH-30115	Chencha	1.1	Wood	1904 \pm 23	72–212 AD
CHOLP3T2D240	RICH-30343	Chencha	2.4	Charcoal	5273 \pm 27	4231–3991 BC
CHOLP3T3D100	RICH-30339	Chencha	1.0	Bulk sample	295 \pm 22	1510–1655 AD
CHOLP3T3D230	RICH-30121	Chencha	2.3	Bulk sample	1832 \pm 22	128–309 AD
CHTSP2T9D290	RICH-30114	Chencha	2.9	Charcoal	11,033 \pm 41	11,132–10,891 BC
CHTSP4T8D200	RICH-30344	Chencha	2.0	Bulk sample	107 \pm 21	1690–1923 AD
CHTSP4T8D300	RICH-30288	Chencha	3.0	Wood	1141 \pm 23	774–989 AD
CHTSP4T8D350	RICH-30335	Chencha	3.5	Bulk sample	3627 \pm 26	2122–1899 BC
CHTSP4T8D400	RICH-30123	Chencha	4.0	Bulk sample	4430 \pm 23	3322–2929 BC
CHTSP5T2D480	RICH-30113	Chencha	4.8	Wood	1911 \pm 22	65–210 AD
CHTSP5T3D340	RICH-30338	Chencha	3.4	Wood	889 \pm 23	1047–1221 AD
DEMP10T2D240	RICH-30336	Dembelle	2.4	Wood	125.41 \pm 0.35	1690–1923 AD
DEMP10T2D310	RICH-30340	Dembelle	3.1	Charcoal	125.13 \pm 0.32	1690–1923 AD
DEMP10T2D400	RICH-30337	Dembelle	4	Wood	147 \pm 22	1669–1728 AD
DEMP10T2D540	RICH-30134	Dembelle	5.4	Charcoal	99 \pm 21	1692–1919 AD
DEMP21T1D300	RICH-30132	Dembelle	3	Wood	26 \pm 21	1697–1910 AD
DEMP21T1D400	RICH-30119	Dembelle	4	Wood	164 \pm 21	1665–1896 AD
DEMP34T1D250	RICH-30116	Dembelle	2.5	Wood	117 \pm 20	1685–1928 AD
DEMP34T1D580	RICH-30345	Dembelle	5.8	Wood	137.94 \pm 0.34	1683–1930 AD

Appendix B

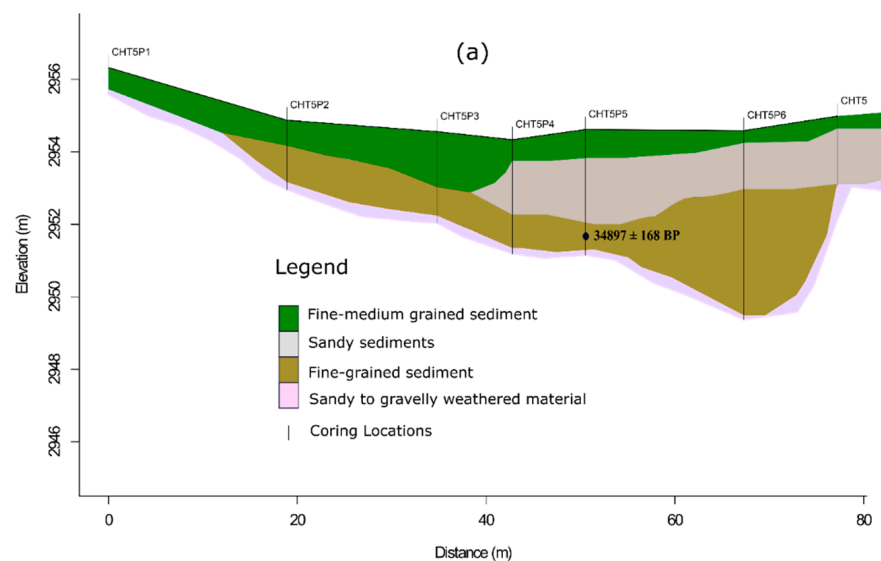


Figure A1. Cont.

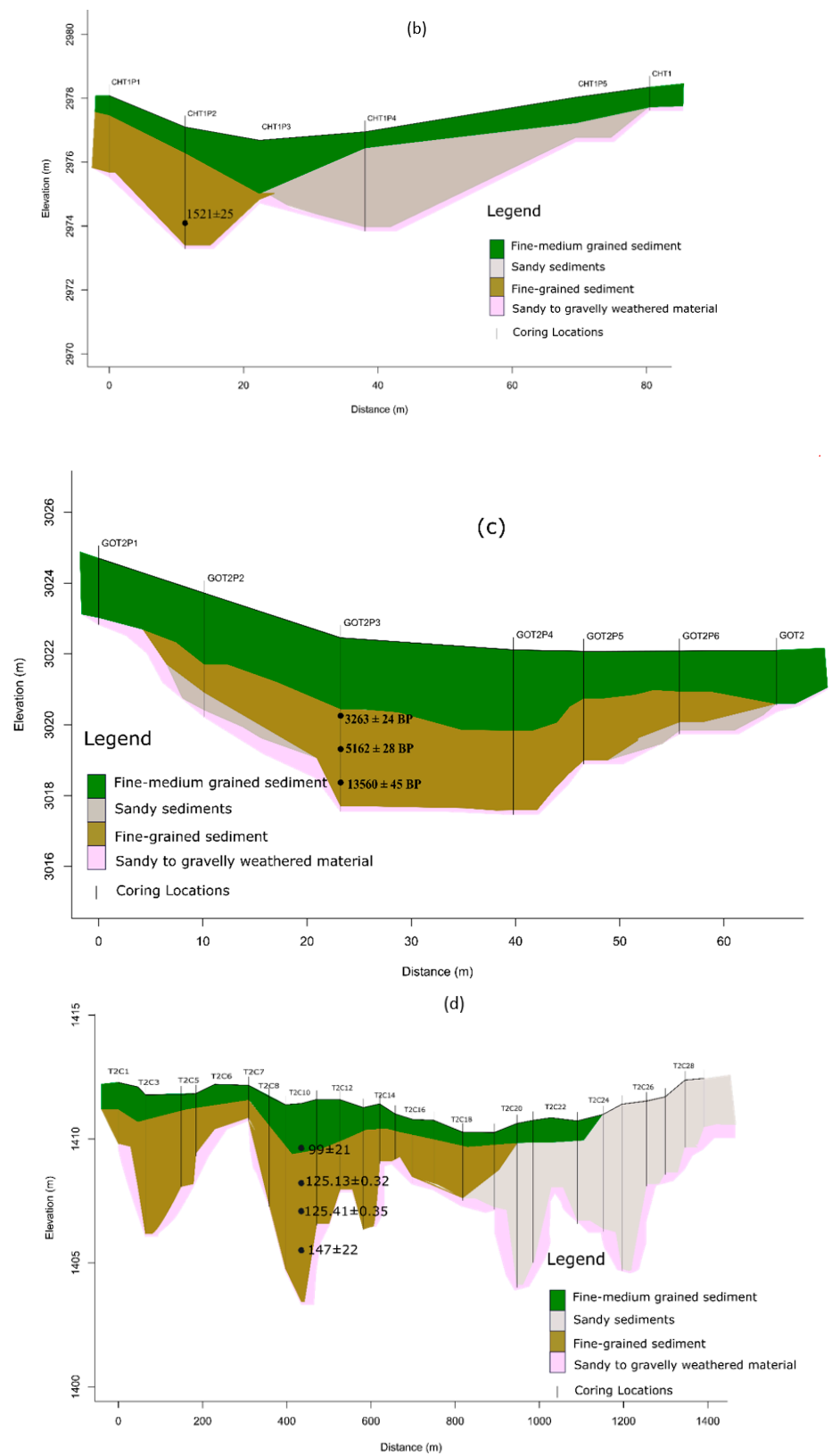


Figure A1. Typical cross-section with indication of the various sedimentary units in the (a–c) Chencha floodplain (d) Dembelle floodplain.

References

1. Trimble, S.W. Decreased rates of alluvial sediment storage in the Coon Creek Basin, Wisconsin, 1975–1993. *Science* **1999**, *285*, 1244–1246. [[CrossRef](#)] [[PubMed](#)]
2. Rommens, T.; Verstraeten, G.; Bogman, P.; Peeters, I.; Poesen, J.; Govers, G.; Van Rompaey, A.; Lang, A. Holocene alluvial sediment storage in a small river catchment in the loess area of central Belgium. *Geomorphology* **2006**, *77*, 187–201. [[CrossRef](#)]
3. Hoffmann, T.; Erkens, G.; Gerlach, R.; Klostermann, J.; Lang, A. Trends and controls of Holocene floodplain sedimentation in the Rhine catchment. *Catena* **2009**, *77*, 96–106. [[CrossRef](#)]
4. Notebaert, B.; Verstraeten, G.; Govers, G.; Poesen, J. Quantification of alluvial sediment storage in contrasting environments: Methodology and error estimation. *Catena* **2010**, *82*, 169–182. [[CrossRef](#)]
5. Notebaert, B.; Verstraeten, G.; Rommens, T.; Vanmontfort, B.; Govers, G.; Poesen, J. Establishing a Holocene sediment budget for the river Dijle. *Catena* **2009**, *77*, 150–163. [[CrossRef](#)]
6. Macklin, M.; Benito, G.; Gregory, K.; Johnstone, E.; Lewin, J.; Michczyńska, D.; Soja, R.; Starkel, L.; Thorndycraft, V. Past hydrological events reflected in the Holocene fluvial record of Europe. *Catena* **2006**, *66*, 145–154. [[CrossRef](#)]
7. Lewin, J.; Macklin, M.G.; Johnstone, E. Interpreting alluvial archives: Sedimentological factors in the British Holocene fluvial record. *Quat. Sci. Rev.* **2005**, *24*, 1873–1889. [[CrossRef](#)]
8. Walling, D.E. Linking land use, erosion and sediment yields in river basins. *Hydrobiologia* **1999**, *410*, 223–240. [[CrossRef](#)]
9. Walling, D.E.; Collins, A.L. The catchment sediment budget as a management tool. *Environ. Sci. Policy* **2008**, *11*, 136–143. [[CrossRef](#)]
10. Tan, Z.; Leung, L.R.; Li, H.Y.; Tesfa, T. Modeling Sediment Yield in Land Surface and Earth System Models: Model Comparison, Development, and Evaluation. *J. Adv. Model. Earth Syst.* **2018**, *10*, 2192–2213. [[CrossRef](#)]
11. Hasholt, B.; van As, D.; Mikkelsen, A.B.; Mernild, S.H.; Yde, J.C. Observed sediment and solute transport from the Kangerlussuaq sector of the Greenland Ice Sheet (2006–2016). *Arct. Antarct. Alp. Res.* **2018**, *50*, S100009. [[CrossRef](#)]
12. Walling, D.E.; Webb, B.W. Erosion and sediment yield: A global overview. *IAHS Publ.* **1996**, *236*, 3–19.
13. Verstraeten, G.; Rommens, T.; Peeters, I.; Poesen, J.; Govers, G.; Lang, A. A temporarily changing Holocene sediment budget for a loess-covered catchment (central Belgium). *Geomorphology* **2009**, *108*, 24–34. [[CrossRef](#)]
14. Hoffmann, T.; Erkens, G.; Cohen, K.M.; Houben, P.; Seidel, J.; Dikau, R. Holocene floodplain sediment storage and hillslope erosion within the Rhine catchment. *Holocene* **2007**, *17*, 105–118. [[CrossRef](#)]
15. Notebaert, B.; Berger, J.; Léopold, J. Characterization and quantification of Holocene colluvial and alluvial sediments in the Valdaine Region (southern France). *Holocene* **2014**, *24*, 1320–1335. [[CrossRef](#)]
16. Zielhofer, C.; Faust, D. Mid- and Late Holocene fluvial chronology of Tunisia. *Quat. Sci. Rev.* **2008**, *27*, 580–588. [[CrossRef](#)]
17. de Moor, J.J.W.; Verstraeten, G. Alluvial and colluvial sediment storage in the Geul River catchment (The Netherlands)—Combining field and modelling data to construct a Late Holocene sediment budget. *Geomorphology* **2008**, *95*, 487–503. [[CrossRef](#)]
18. Notebaert, B.; Verstraeten, G.; Vandenbergh, D.; Marinova, E.; Poesen, J.; Govers, G. Changing hillslope and fluvial Holocene sediment dynamics in a Belgian loess catchment. *J. Quat. Sci.* **2011**, *26*, 44–58. [[CrossRef](#)]
19. Marston, R.A.; Bravard, J.P.; Green, T. Impacts of reforestation and gravel mining on the Malnant River, Haute-Savoie, French Alps. *Geomorphology* **2003**, *55*, 65–74. [[CrossRef](#)]
20. Dugar, B.; Verstraeten, G.; Notebaert, B.; Bakker, J. Holocene environmental change and its impact on sediment dynamics in the eastern mediterranean. *Earth-Sci. Rev.* **2011**, *108*, 137–157. [[CrossRef](#)]
21. Darbyshire, I.; Lamb, H.; Umer, M. Forest clearance and regrowth in northern Ethiopia during the last 3000 years. *Holocene* **2003**, *13*, 537–546. [[CrossRef](#)]
22. Nyssen, J.; Poesen, J.; Moeyersons, J.; Deckers, J.; Haile, M.; Lang, A. Human impact on the environment in the Ethiopian and Eritrean highlands—A state of the art. *Earth-Sci. Rev.* **2004**, *64*, 273–320. [[CrossRef](#)]
23. Arthur, J.W.; Curtis, M.C.; Arthur, K.J.W.; Coltorti, M.; Pieruccini, P.; Lesur, J.; Fuller, D.; Lucas, L.; Conyers, L.; Stock, J.; et al. The Transition from Hunting–Gathering to Food Production in the Gamo Highlands of Southern Ethiopia. *Afr. Archaeol. Rev.* **2019**, *36*, 5–65. [[CrossRef](#)]
24. Coltorti, M.; Pieruccini, P.; Arthur, K.J.W.; Arthur, J.; Curtis, M. Geomorphology, soils and palaeosols of the Chencha area (Gamo Gofa, south western Ethiopian Highlands). *J. Afr. Earth Sci.* **2019**, *151*, 225–240. [[CrossRef](#)]
25. Bronk Ramsey, C.; Michael, D.; Sharen, L.; Nakagawa, T.; Staff, R.A. Developments in the Calibration and modeling of radiocarbon dates. *Radiocarbon* **2010**, *52*, 953–961. [[CrossRef](#)]
26. Hoffmann, T.; Lang, A.; Dikau, R. Holocene River activity: Analysing ¹⁴C-dated fluvial and colluvial sediments from Germany. *Quat. Sci. Rev.* **2008**, *27*, 2031–2040. [[CrossRef](#)]
27. Chiverrell, R.C.; Thorndycraft, V.R.; Hoffmann, T.O. Cumulative probability functions and their role in evaluating the chronology of geomorphological events during the Holocene. *J. Quat. Sci.* **2011**, *26*, 76–85. [[CrossRef](#)]
28. Dugar, B.; Verstraeten, G.; D’Haen, K.; Bakker, J.; Kaptijn, E.; Waelkens, M. Sensitivity of the Eastern Mediterranean geomorphic system towards environmental change during the Late Holocene: A chronological perspective. *J. Quat. Sci.* **2012**, *27*, 371–382. [[CrossRef](#)]
29. Rommens, T.; Verstraeten, G.; Lang, A.; Poesen, J.; Govers, G.; Van Rompaey, A.; Peeters, I. Soil erosion and sediment deposition in the Belgian loess belt during the Holocene: Establishing a sediment budget for a small agricultural catchment. *Holocene* **2005**, *15*, 1032–1043. [[CrossRef](#)]

30. Assefa, E.; Bork, H.R. Deforestation and forest management in Southern Ethiopia: Investigations in the Chench and Arbaminch areas. *Environ. Manag.* **2014**, *53*, 284–299. [[CrossRef](#)]
31. Tsige, G. Holocene Environmental History of Lake Chamo, South Ethiopia. Ph.D. Thesis, Universität zu Köln, Cologne, Germany, 2015.
32. Kiage, L.M.; Liu, K.B. Late Quaternary paleoenvironmental changes in East Africa: A review of multiproxy evidence from palynology, lake sediments, and associated records. *Prog. Phys. Geogr.* **2006**, *30*, 633–658. [[CrossRef](#)]
33. Njagi, D.M.; Routh, J.; Olago, D.; Gayantha, K. A multi-proxy reconstruction of the late Holocene climate evolution in the Kapsabet Swamp, Kenya (East Africa). *Paleogeography Palaeoclimatol. Paleoecol.* **2021**, *574*, 110475. [[CrossRef](#)]
34. FAO. *Ethiopian Highlands Reclamation Study*; Final Report of Food and Agricultural Organization; FAO: Rome, Italy, 1986.
35. Hurni, H. Erosion–productivity–conservation systems in Ethiopia. In Proceedings of the IV International Conference on Soil Conservation, Maracay, Venezuela, 3–9 November 1985; pp. 654–674.
36. Hurni, H. Degradation and Conservation of the Resources in the Ethiopian Highlands. *Mt. Res. Dev.* **1988**, *8*, 123–130. [[CrossRef](#)]